7. ANKARA INTERNATIONAL AEROSPACE CONFERENCE
11-13 September 2013 - METU, Ankara TURKEY

AIAC-2013-021

PRELIMINARY DESIGN OF A TRANSONIC FAN FOR LOW BY-PASS TURBOFAN ENGINE

Mohamed A. Aziz[1]
Institute of Aviation Engineering and Technology
Giza, Egypt

Farouk M.Owis[2]
Cairo University
Giza, Egypt

Mohamed.M.Abdelrahman [3]
Cairo University
Giza, Egypt

ABSTRACT

Design optimization of axial compressors using numerical simulations requires huge computational efforts. Therefore, the design process needs to be started from a reasonable design point. In the current study, a design tool is developed for the preliminary design of transonic compressors using different correlations of cascade experimental data for the shock losses and the deviation angle. A parametric study is performed to select the design parameters for optimum fan performance in terms of efficiency and surge margin. The designed fan is tested during off design operation and simulated numerically using computational fluid dynamics to verify the developed design tool. The numerical simulations of designed fan show good agreement with the preliminary design results.

INTRODUCTION

Transonic axial flow compressors are widely used in recent aircraft engines to obtain maximum pressure ratios per stage. High stage pressure ratios are important to reduce the engine weight, size and operational costs. Performance of transonic compressors has reached a high level but further improvements are required by engine manufacturers. A small increment in efficiency can result in huge savings in fuel costs and this is considered a key factor for the product success.

Important analytical and experimental researches in the field of transonic compressors were carried out since 1960's. A considerable contribution for the new developments and designs is the progress made in optical measurement techniques and computational methods, leading to a deeper understanding of the loss mechanisms of supersonic relative flow in compressors (e.g. [Hah & Reid 1992]; [Ning & Xu, 2001]; [Puterbaugh et al., 1997]; [Strazisar, 1985]; [Mdouki & Gahmousse, 2012]). The flow field that develops inside a transonic compressor rotor is extremely complex and presents many challenges to compressor designers, who have to deal with several and concurring flow features such as shock waves, intense secondary flows, shock/boundary layer interaction, etc., inducing energy losses and efficiency reduction.

With advances in Computational Fluid Dynamics (CFD) and computer hardware, CFD has become an integral part of the blade design process. CFD has been employed to cut aerodynamic design cost and time scales by reducing the number of required experiments. A preliminary design is therefore required as a prelude to the optimization problem. The design process for the compressor encompasses the following steps; choice of rotational speeds, determination of the number of stages, calculation of the air angles, the blade losses at the mean radius, variation of the air angles from root to tip. In addition, selection of blade geometry is done by performing a parametric study over a number of variables affecting the compressor performance. Calculations of the rotor map at the off design conditions are needed to judge the selected deign parameters.

[1] Ass. Teacher. İn Aerospace Department, Email: mhessen_aziz@yahoo.com
[2] Ass. Prof. İn Aerospace Department, Email: fowis@eng.cu.edu.eg
[3] Prof. İn Aerospace Department, Email: Dr_madbouli@hotmail.com

Important analytical and experimental studies in the field of transonic compressors have been carried out since 1960's. [Miller et al. 1961] have made a good advancement in the art of transonic compressors. Different correlations for a variety of rotors operating over a wide range of conditions are presented. The theoretical analysis described in [Wennerstrom 2000] and [Wu 1952] provides a general description of the design methodology for axial fans.

The preliminary design and off-design of turbomachines require experimental and theoretical correlations to estimate the pressure losses, incidence angle at the design and the deviation angle. Different pressure loss models including the shock loss models are suggested for the preliminary design of transonic compressors. A new model is presented by [Wennerstrom and Puterbaugh 1984] for predicting the shock loss through a transonic or supersonic compressor blade row operating at peak efficiency. This model is different from the classical [Miller 1961] normal shock model. It takes into account the span wise obliquity of the shock surface due to leading-edge sweep, blade twist, and solidity variation. [Freeman and Cumpsty 1992] used a simple model to calculate the flow in transonic compressor blades. The method addresses the common irreversible deceleration and compression that takes place when a shock stands ahead of the blade leading edge. This model is able to predict the loss creation in the inlet region. [Puterbaugh et al. 1997] presented an analysis of the effectiveness of a three-dimensional shock loss model used in transonic compressor rotor design. The model is used for the design of an aft-swept, transonic compressor rotor. This shock loss model is developed to account for the benefit gained with three-dimensional shock sweep.

[Strazisar 1985] investigated several flow phenomena, including flow field periodicity, rotor shock oscillation, and rotor shock system geometry in a transonic low aspect ratio fan rotor using laser anemometry. [Schreiber and Tweedt 1987] suggested a new method to determine the shock loss and profile loss portions of the overall loss from actual measurement. The method applied on L030-4 and L030-6 cascades over a range of operating conditions to form an excellent basis for validating a shock loss model. [Konig et al. 1996] used new blading concepts to improve loss and deviation angle correlations. The model incorporates several elements and treats blade-row flows having subsonic and supersonic inlet conditions established for DCA bladings and modified to reflect the flow situation in blade rows having arbitrarily designed blades including precompression blades. The steady loss increases from subsonic to supersonic inlet-flow velocities demonstrates the matched performance of the different correlations of the new model.

There are many correlations dealing with the incidence angle and deviation angle at the design and off design conditions. The minimum loss incidence angle given by [Lieblein 1965] considers the viscous effects on two-dimensional incompressible flow about compressor blade profiles in cascade. [Hearsey 1970] developed the stream line curvature method by using empirical cascade data to determine low-speed, minimum loss –incidence, deviation and loss. In addition, the deviation angle at the design conditions is given by [Carter's 1950]. [Cetin, et al. 1987] recommended a modification to Carter's rule to account for underestimation of the deviation at design conditions.

Design validation and optimization of transonic compressors are done using the numerical solution of the turbulent flow equations. [Hah and Reid 1992] conducted a numerical study based on the three-dimensional Reynolds-averaged Navier–Stokes equation to investigate the detailed flow physics inside a transonic compressor. Three-dimensional shock structure, shock-boundary layer interaction, flow separation, radial mixing, and wake development are all investigated at the design and off-design conditions. [Ning and Xu 2001], made a numerical investigation of transonic compressor rotor flow using an implicit 3D flow solver with one-equation Spalart-allmaras turbulence model.

A closer look at the current trend in the design parameters for axial flow transonic compressors shows that, especially for civil aircraft engines, the inlet relative Mach number at the rotor tip is limited to 1.3 to maintain high compressor efficiency. This value may increase to 1.6 in some high speed rotors as suggested by [Law and Puterbaugh 1988]. Today's high efficiency transonic axial flow compressors give a total pressure ratio in the order of 1.7-1.8 per stage. These high pressure ratios can be obtained by combining high rotor speeds, tip speed in the order of 500 m/s, and high stage loadings $2\Delta h/u^2$ in the order of 1.0 as suggested by [Biollo and Benini 2011]. The number of stages is related to the stage total temperature rise. The temperature rise per stage for the current subsonic compressors is limited to values between 10- 30 K and 45 -55 K for transonic stages according to [Saravanamuttoo and et. al. 2001].

The objective of the current study is to develop a reliable low fidelity-design tool for the design of transonic compressors that can be used as an initial geometry for the numerical simulations. A parametric study of compressor blade geometry is performed to achieve optimum design and off-design operations in terms of fan efficiency and surge margin. There are different types of blade geometries used in axial compressors such as double circular arc (DCA), multiple circular arcs (MCA), pre-compression, and controlled diffusion. The surfaces of the blades for the last two types are specifically designed to achieve certain distribution of flow properties through the rotor for specific applications. The (MCA) profile is considered a good choice to design compressor blades during the preliminarily steps.

There are certain blade characteristics that are generally regarded as beneficial to achieving compression in the transonic regime in terms of solidity, aspect ratio, stagger angle and camber angle. Stagger angle is particularly an important parameter when supersonic flows are involved because of the direct effect on passage area, and therefore on maximum mass flow rate [Cumpsty and Nicholas 1989]. Therefore, it is necessary to perform a parametric study during the preliminary design to select the suitable parameters.

One of the most important airfoil design parameters affecting the aerodynamics of transonic blading is the chord wise location of maximum thickness. An experimental and numerical evaluation of two versions of a low aspect ratio transonic rotor by [Wadia and Law, 1993] showed that more aft position of maximum thickness is preferred for the best high speed performance. Similar results can be found in a recent work by [Chen et al. 2007] describing an optimization methodology for the aerodynamic design of a transonic compressor blading and showing how the thermal loss coefficient decreases with increasing the maximum thickness location for all the sections from hub to tip. Also the airfoil thickness has been showed to have a significant impact on the aerodynamic behavior of transonic compressor rotors, as observed in an investigation on airfoil thickness effects by [Suder et al. 1995]. The leading edge radius (LER) reduction has a beneficial effect on the bow shock loss as mentioned by [Boyer 2001]. He found that an increase in detached bow shock loss from 10% of total shock loss to over 60% of shock loss as the LER increased from 0.01 to 0.1 inches. Transonic compressor blades tend to have a small amount of camber (ϕ) overall, to reduce the strength of the passage shock and lower the risk of a shock induced boundary-layer separation [König 1996].

.

MATHIMATICAL MODEL

The design process for the fan will encompass the following steps:

1. Selection of rotational speeds, inlet hub to tip radius ratios, stagger angle and geometrical parameters defining the blade geometry.
2. Determination of number of stages using an assumed overall fan efficiency.
3. Calculation of the flow angles, blade angles and losses at mean section.
4. Calculation of stages efficiencies and pressure ratios.
5. Performing off design study for the calculated design parameters.
6. Performing a parametric study and select the most promising design.

<u>Choice of the Design Parameters</u>. The choice of the rotational speed is limited by the blade tip speed. The base line case data which is used in the design process with an assumed polytropic efficiency of 0.9 is presented in Table 1.

Table 1: Base line data of the selected case.

Requirements		Inlet Conditions		Selected Parameters	
Mass flow rate	120 kg/sec	Total inlet temperature	300 K	N (r.p.m)	<10500
Fan pressure ratio	2.6	Total inlet pressure	101.325 kPa	Hub to tip ratio	0.2-0.7
				Diffusion Factor	<0.55
				Inlet axial Mach Number	0.7

An initial estimation of the number of stages for equal total temperature rise of the stages indicates that 3 stages are required to obtain the required overall pressure ratio. This number of stages may be changed as the design parameters are changed to obtain suitable fan performance. A closer look on a transonic compressor blading showed that MCA blading is the compromise solution between the number of variables and the computational effort required for the parametric study during the preliminary design steps. The defining parameters for this type of blading are described in Fig. 1. Four circular arcs, two of them are drawn from the leading edge and the other two are drawn from the trailing edge. The circular arcs are drawn tangent to the maximum thickness circle to construct an MCA-profile blade. The blade LE is on the right of Fig. 1.

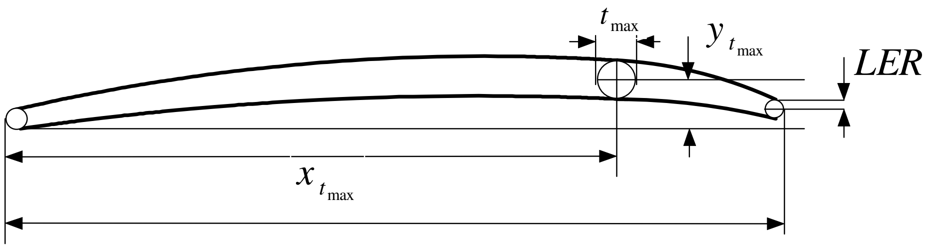

Figure 1: Geometrical descriptions of the five parameters that Define MCA

Experimental Data and Fan Loss Models. There are many correlations describing the components which lead to the estimation of total losses and hence the rotor performance in terms of fan pressure ratio and efficiency. Several studies are conducted to validate the most suitable set of correlations with available experimental data. [Cahill 1997] performed a valuable comparison with a large variety of correlations for two transonic rotors (NASA Rotor 1-B and NASA Rotor 35). The profile loss model by [Hearsey 1970] and the shock loss model suggested by [Koch and Smith 1976] have accurate predictions compared to the experimental data of Rotor 35.

The Design Incidence and Deviation Models. The design incidence is calculated using the following correlation of [Lieblein 1965]:

$$i^*_{2D} = (K_i)_{sh}(K_i)_t(i_0)_{10} + n\theta \qquad (1)$$

Where,

$(K_i)_{sh}$ = correction for profile shape different from NACA 65 airfoil profiles.

$(K_i)_t$ = correction for maximum blade thickness

$(i_0)_{10}$ = zero-camber incidence angle for ten-percent thick 65-series blades

n = slope factor

θ = blade camber angle

[Çetin et al. 1987] suggested the following inlet Mach number correction to the design incidence i^*_{2D} :

$$i^*_{cor} = i^*_{2D} + 5.738 + 1.3016 M_{r1} \qquad (2)$$

The modified Carter correlation by [Çetin et al. 1987] is used to calculate the deviation angle at the design conditions.

$$\delta^*_{carter} = (K_\delta)_{sh}(K_\delta)_t(\delta_0)_{10} + \frac{m_{\sigma=1}}{\sigma^b}\theta \qquad (3)$$

Where,

$(K_\delta)_{sh}$ = correction for thickness distribution

$(K_\delta)_t$ = correction for maximum blade thickness

$(\delta_0)_{10}$ = zero-camber deviation angle for ten-percent thick 65- series blades

$m_{\sigma=1}$ = rate of change of deviation angle with camber angle for σ = 1.0

σ^b = term accounting for variable influence of solidity associated with β_1

The constants $m_{\sigma=1}$ and the solidity exponent b are functions of the inlet flow angle β_1. Çetin et al. proposed a correction to Carter's Rule based on the stagger angle ζ as follows,

$$\delta_{\text{modified}} = \frac{(\varepsilon - i)\, m\, \sqrt{s/c}}{1 - m\, \sqrt{s/c}} \tag{4}$$

Where the constant m is given by the following relation:

$$m = \left(0.219 + 0.0008916\zeta + 0.00002708\zeta^2\right) \times \left(2\frac{a}{c}\right)^{2.175 - 0.03552\zeta + 0.0001917\zeta^2} \tag{5}$$

Calculation of the Off-Design Deviation. Correlation suggested by [Creveling 1968] is used to calculate the deviation angle at the off-deign as follows,

$$\frac{\delta - \delta^*}{\Delta\beta^*} = f(x) \tag{6}$$

$$f(x) = \begin{cases} -0.809\times10^{-3} + 0.5588x - 0.2928x^2 & x \geq 0 \\ 0.1191\times10^{-3} + 0.48x - 0.3452x^2 & x < 0 \end{cases} \tag{7}$$

Where, $x = \dfrac{i - i^*}{\Delta\beta^*}$

Pressure Loss Models at the Design Conditions. Individual loss components for highly transonic fans can be classified into three main categories as suggested by [Koch and Smith 1976]:

- Profile loss – includes blade boundary layer and wake
- Shock loss – due to non-isentropic shock process in the primary (or core) flow
- Secondary loss – includes passage secondary flows and end-wall interactions between annulus boundary layer and blade rows (tip gap flows and hub vortices)

$$\omega_{\min} = \omega_{profile} + \omega_{shock} + \omega_{secondary} + \omega_{tip\ clearance} + \omega_{annulus} \tag{8}$$

In many cases, the profile loss remains approximately constant over the working range of highly transonic blade sections as explained by [Boyer 2001] with two examples (the work of [Bloch, et al., 1996], and [König, et al., 1996]). For designs with M1rel > 1.4, the shock loss can be an order of magnitude greater than the profile loss. As the tip loads up, both the shock loss and secondary loss increase. As the back pressure increases, the shock moves upstream, becoming more normal to the flow and further detached from the leading edge.

Profile loss (blade section boundary layer and wake) $\omega_{profile}$ is determined using the method of [Koch and Smith 1976]. An equivalent diffusion factor, D_{eq}^* is defined as the product of three velocity ratios,

$$D_{eq}^* = \frac{W_{\max}}{W_{TE}} = \frac{W_P}{W_1} \cdot \frac{W_{\max}}{W_P} \cdot \frac{W_1}{W_{TE}} \tag{9}$$

Where,

$W_{\max}$ = maximum suction surface velocity

W_{TE} = trailing edge velocity

W_P = mean passage velocity in blade passage throat region

Relationships are derived for the first two terms on the right hand side of equation (9). The third term can be calculated immediately from the inlet and exit velocity triangles of the rotor. The ratio of passage throat velocity to inlet velocity was obtained from the following four equations:

$$\frac{W_P}{W_1} = \left[(\sin\beta_1 - 0.2445\sigma\Gamma^*)^2 + \left[\frac{\cos\beta_1}{A_P^*\left(\frac{\rho_P}{\rho_1}\right)} \right]^2 \right]^{\frac{1}{2}} \qquad (10)$$

$$\frac{\rho_P}{\rho_1} = 1 - \frac{M_{1n}^2}{1-M_{1n}^2}\left(1 - A_P^* - 0.2445\frac{\tan\beta_1}{\cos\beta_1}\sigma\Gamma^*\right) \qquad (11)$$

$$A_P^* = \left[\frac{1-0.4458\sigma t_{\max}/c}{\cos(\frac{\beta_1+\beta_2}{2})} \right]\left(1 - \frac{A_{a1}-A_{a2}}{3A_{a1}}\right) \qquad (12)$$

$$\Gamma^* = \frac{R_1 W_{u1} - R_2 W_{u2}}{\bar{R}\ \sigma W_1} \qquad (13)$$

Where,

Γ^* = blade circulation parameter

A_P^* = annulus area contraction ratio from cascade inlet to passage throat

A_a = annulus area

M_{n1} = axial Mach number at station 1

The ratio of maximum suction surface velocity to passage velocity is obtained from the following equation:

$$\frac{W_{\max}}{W_P} = 1 + 0.7688\left(t_{max}/c\right) + 0.6024\Gamma^* \qquad (14)$$

Using Lieblein definitions, we have the following relation for the local diffusion factor:

$$D^* = D_{eq}^*\frac{W_2}{W_1} - \frac{W_2}{W_1} \qquad (15)$$

The profile loss coefficient for subsonic stream tubes is given by,

$$\omega_{profile} = \frac{2\sigma}{\cos\beta_2^*}\left(\frac{\theta}{L}\right) \qquad (16)$$

where θ is the wake momentum thickness.

A correlation suggested by [Lakshminarayana and Horlock, 1963] is used to determine the losses in the end-wall. The secondary flow loss and the annulus boundary layer loss are calculated using correlations discussed by [Horlock 1973].

Pressure Loss Models at the off-design conditions. The following correlation for off design profile loss by [Çetin et al. 1987] is used:

$$\omega = \omega^* + c_m\left(i - i^*\right)^2 \qquad (17)$$

where,

$$c_m = \begin{cases} 0.02845M - 0.01741 \\ 0.00363M - 0.00065 \end{cases} \quad for \quad \begin{matrix} i - i^* < 0 \\ i - i^* \geq 0 \end{matrix} \qquad (18)$$

c_m is a correction coefficient for inlet Mach number.

The method of [Bloch, 1996] that is modified by [Boyer, 2001] provides the basis for the present shock loss model. Prediction of off-design shock losses requires a priori knowledge of the shock structure and Mach number. The method of [Moeckel, 1949], modified by [Bloch, 1996], is used to determine the shape of the detached leading edge shock and detachment distance. The method requires specification of the inlet relative Mach number M_{1rel} and blade leading edge radius (LER). An evaluation method of the bow shock is discussed by [Bloch, 1996]. An estimate of the total pressure loss due to the detached bow portion of the shock is obtained for a specified shock shape and location. The total pressure drop is estimated from the following relation:

$$\frac{P_{0A}}{P_{01}} = 1 - \frac{\int_0^\infty \left(1 - \frac{P_{0A}}{P_{01}}\right) dy}{s \cos(\xi)} \qquad (19)$$

where P_{0A} is the total pressure downstream the bow shock.

This condition limited by the Mockoel hyperbola lies upstream the next adjacent blade leading edge as shown in Fig. (2). If the obliqueness of the shock increased, then the bow shock will intersect with the pressure side of the adjacent blade and then is reflected again into the passage. Figure (3) shows an increase of bow shock obliqueness due to Mach number increase and LER decrease which may be the case at the mean section (to the left) and at tip section (to the right). The total pressure loss due to the bow shock then is estimated as follows,

$$\frac{P_{0A}}{P_{01}} = 1 - \frac{\int_0^{s\cos(\xi)} \left(1 - \frac{P_{0A}}{P_{01}}\right) dy}{s \cos(\xi)} \qquad (20)$$

where P_{0A}/P_{01} is obtained from the oblique shock theory applied locally as the integration proceeds.

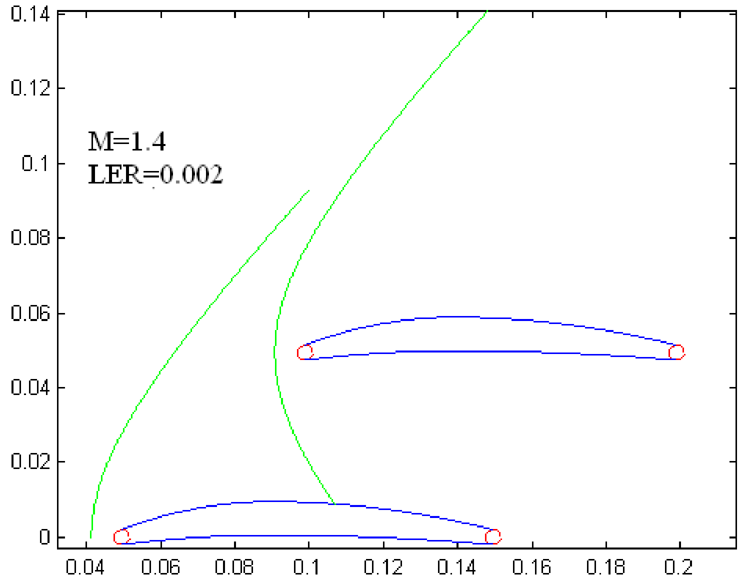

Figure 2: Identical wave pattern for two adjacent case blades

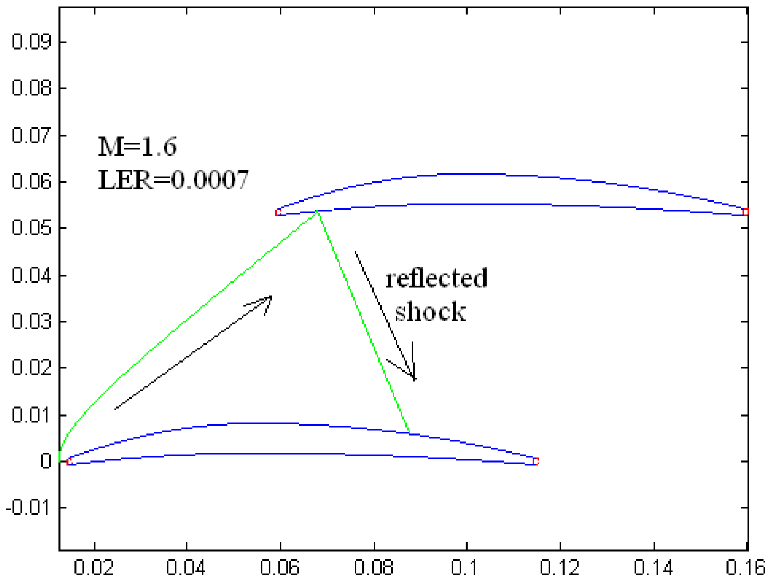

Figure 3: Wave pattern for two adjacent case blades where the Mach number increases and LER decreases.

$$\frac{P_{0A}}{P_{01}}=\left[\frac{(\gamma+1)M_{1,norm}^{2}}{(\gamma-1)M_{1,norm}^{2}+2}\right]^{\frac{\gamma}{\gamma-1}}\left[\frac{\gamma+1}{2\gamma M_{1,norm}^{2}-(\gamma-1)}\right]^{\frac{1}{\gamma-1}} \quad (21)$$

$$M_{1,norm}=M_{1}\sin(\psi) \quad (22)$$

$$\tan\psi=\frac{\sqrt{x_0^2+\left(M^2-1\right)y^2}}{\left(M^2-1\right)y} \quad (23)$$

The spatial increment for integration is chosen to be a small value as follows,

$$dy=\frac{y_{sonic}}{10} \quad (24)$$

where y_{sonic} is the distance from the blade mean camber line to the sonic point on the shock. Eq. (21) is integrated until the following condition is satisfied:

$$(1.0-\frac{P_{0A}}{P_{01}})\leq 0.0005 \quad (25)$$

For the first passage shock, an approximation of first passage shock between the low and medium back pressure regimes according to [Bloch, 1996] is described in figure (4). The decrease in total pressure caused by this shock is mass averaged as follows,

$$\frac{\bar{P}_{02}}{P_{0A}}=\frac{\int_B^C \rho V_x \frac{P_{02}}{P_{0A}}dy}{\int_B^C \rho V_x\, dy} \quad (26)$$

where, P_{02}/P_{0A} is obtained from equation (21) of the oblique shock theory. The integration steps are determined by equally dividing the axial distance between the blade suction surface at the first captured Mach wave (point A) and at the passage shock intersection point (point C). At each point along the blade surface, the Mach number is calculated as a Prandtl-Meyer expansion from the upstream condition and the Mach lone is extended to the passage shock.

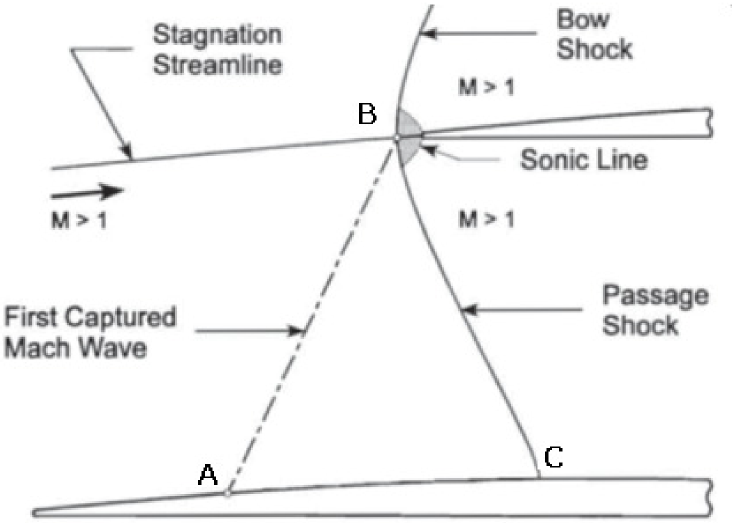

Figure 4: Approximation of first passage shock [Bloch 1996]

If the Mach number directly behind the first shock, M_B, is greater than unity, then a second normal shock is formed. Equation (21) can be used with ψ = 90 degrees to get the total pressure loss across this passage shock. At near shock operation the method of [König, et al., 1996] is used to estimate the Mach number directly upstream of the second shock which is assumed to be at the trailing edge of the passage. The following exit-to-entrance area ratio equation is defined by König et al.:

$$\frac{A_J}{A_B} = 0.499 M_B + 0.501 + C_{ar} \qquad (27)$$

where, C_{ar} = 0.0774 for MCA or wedge sections.

[Boyer 2001] suggests that if the Mach number behind the first shock, M_B in Fig. (6), is subsonic, then the area ratio defined by Equation (27) is assumed to be the critical area ratio, A_J / A^* (i.e., M_B = 1.0). This assumption introduces negligible error, as the existence of the downstream second shock must imply a reacceleration to supersonic velocity. If M_B is supersonic, then the area ratio can be obtained from the compressible flow theory.

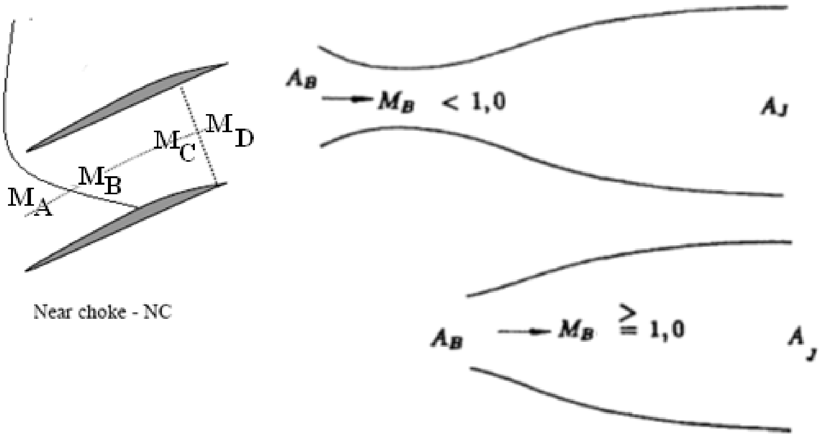

Figure 5: Assumed blade passage contours at Near-choke operating condition [Konig et al.,1996]

$$\frac{A_B}{A^*}=\frac{1}{M_B}\left[\frac{2}{\gamma+1}\left(1+\frac{\gamma-1}{2}M_B^2\right)\right]^{\frac{\gamma+1}{2(\gamma-1)}} \qquad (28)$$

An equation for A_J / A^* can be obtained by combining equations (27) and (28). Then the Mach number just upstream of the second shock M_C can be obtained knowing the critical area ratio.

Preliminary Design Results. A parametric study is performed to investigate the effect of different design parameters on the fan performance and to choose parameters such as the rotational speed, blade geometry parameters and the stagger angle of the rotor and stator. The fan performance is computed in terms of the surge margin, fan efficiency and pressure ratio at the design and off-design conditions. The results indicate that small leading edge radius produces higher rotor efficiency and high pressure ratio.

However, the fan performance shows less sensitivity to changes in the leading edge radius compared with the other geometrical parameters. The effect of the blade shape on the fan performance is presented in figures (6) through (8). The parameters of the blade geometry are selected such that minimum number of stages with maximum isentropic efficiency is obtained and the fan produces the required pressure ratio. The effect of the rotor stagger angle on the stage efficiency and pressure ratio is introduced in Fig. (9). Maximum isentropic efficiency of the rotor is obtained for a stagger angle of 39^o. At this stagger angle of the rotor, the stator has an optimum efficiency at a stagger angle of 17.5^o while the maximum pressure ratio is obtained at a stagger angle of 22.5^o for the stator.

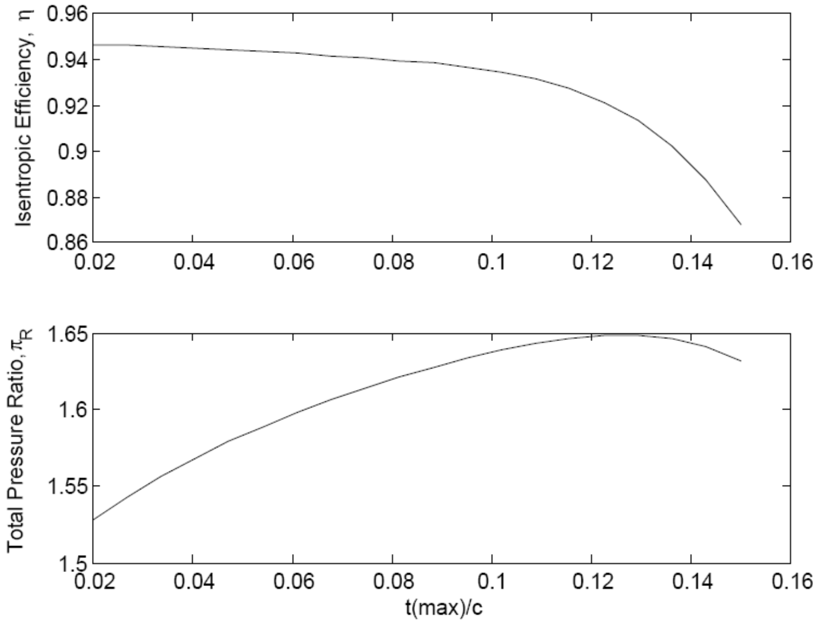

Figure 6: Variation of the total pressure ratio and isentropic efficiency with the changes in blade geometry ($t_{(max)}/c$)

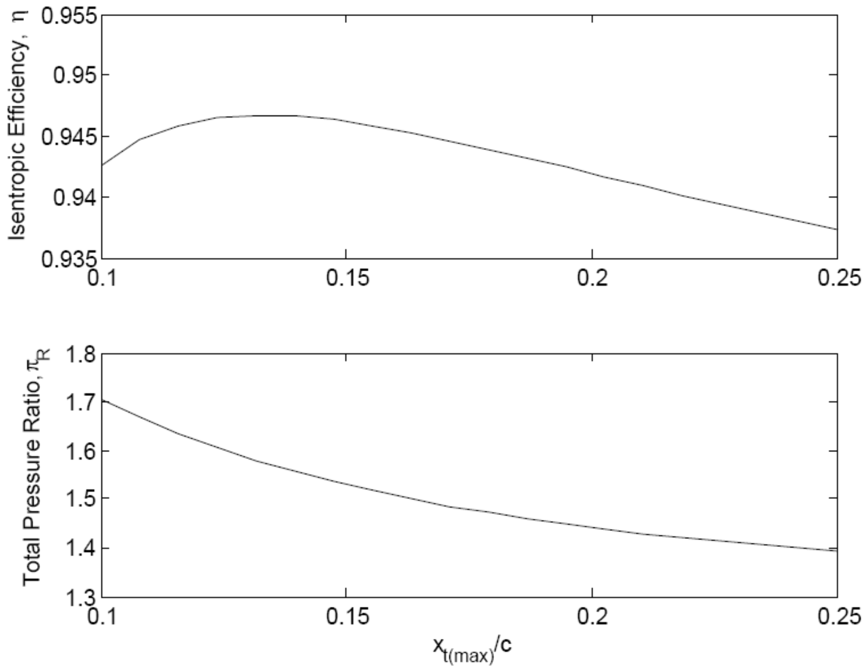

Figure 7: Variation of the total pressure ratio and isentropic efficiency with the changes in blade geometry ($x_{t(max)}/c$).

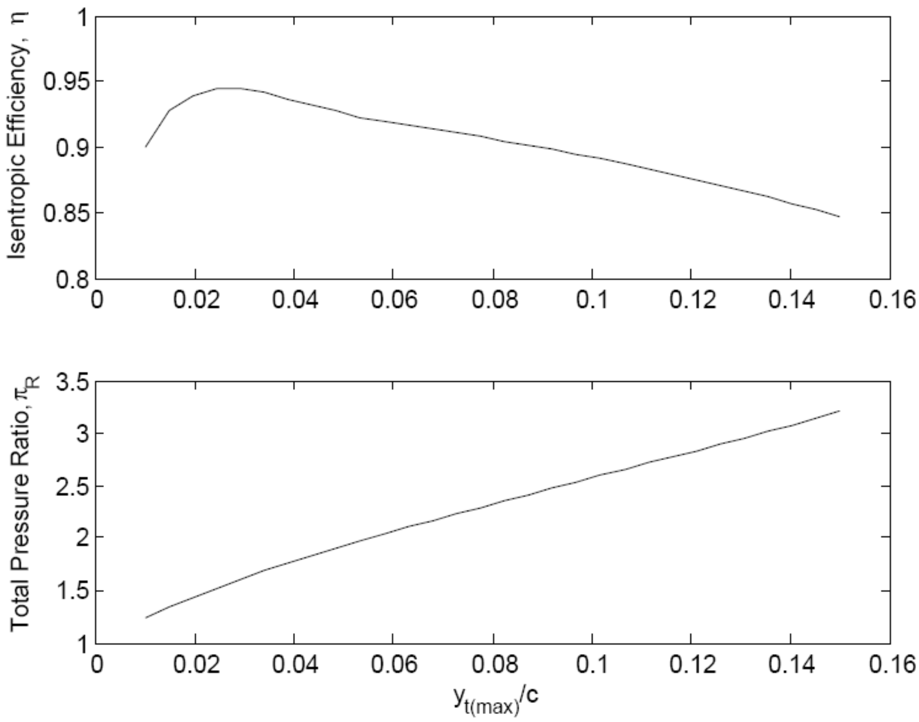

Figure 8: Variation of the total pressure ratio and isentropic efficiency with the changes in blade geometry ($y_{t(max)}/c$).

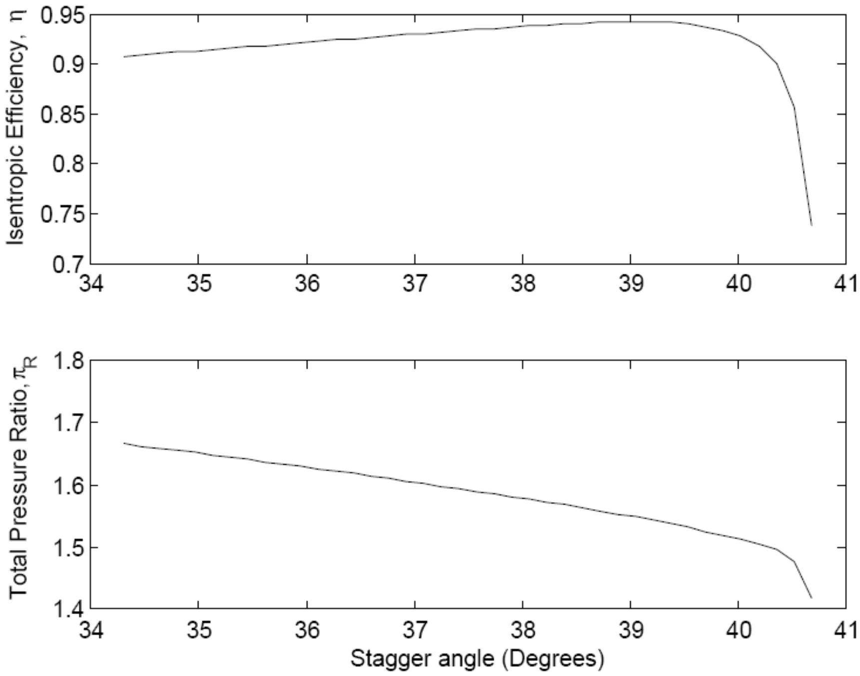

Figure 9: Variation of the total pressure ratio and isentropic efficiency with changes in rotor stagger angles.

The inlet to the first rotor of the fan has the largest annulus area and consequently the first rotor has the largest tip radius. Therefore, the rotational speed is limited by the blade tip speed of the first rotor which is selected to be 450 m/s. The rotational speed has a maximum value of 10200 rpm. Although, the isentropic efficiency and the total pressure ratio of the stage increase by increasing the rotational speed, the surge margin decreases as shown in Fig. (12). Limiting the surge margin to 8.5% yields a rotational speed of 9800 rpm.

The fan design parameters are selected such that the fan will have a maximum efficiency at the specified constraints of 8.5% surge margin and a maximum tip speed of 450 m/s. The results indicate that the minimum number of stages required to obtain a fan pressure ratio of 2.6 are three stages.

The pressure ratios of three stages at the selected deign parameters are 1.55, 1.36 and 1.25. The parameters selected for the preliminary design are presented in Table 2. The variation of the annulus area in the stages is shown in figure (11). The annulus area decreases along the fan because the axial velocity is kept constant throughout the fan at the design conditions.

(A)

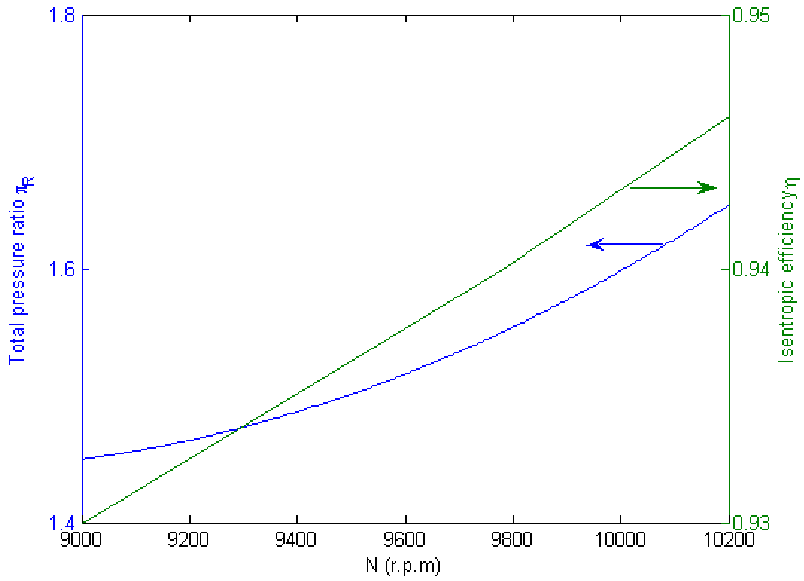

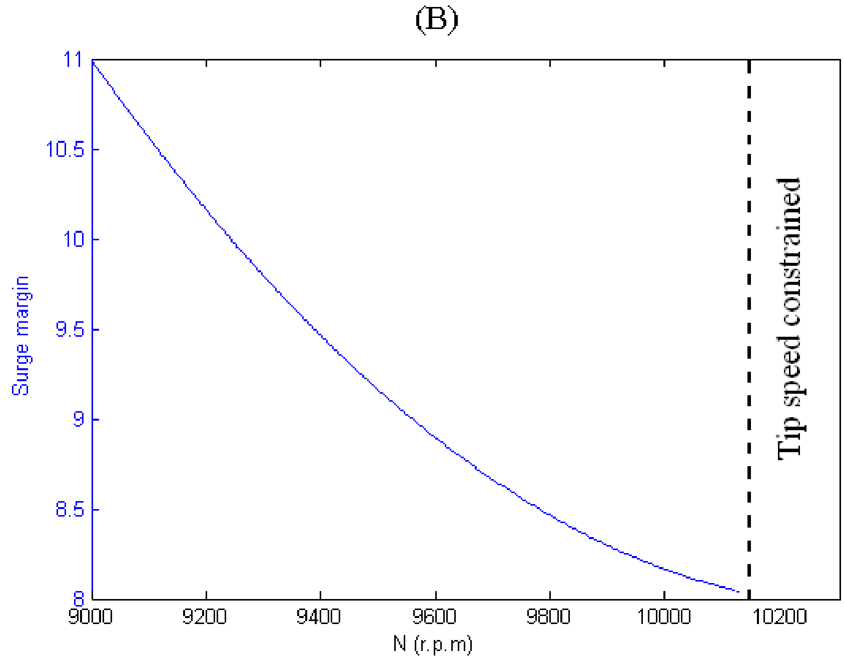

Figure 10: The effect of the rotational speed on rotor performance parameters.

TABLE 2: Preliminary design parameters

Parameter	First Stage		Second Stage		Third Stage	
	Rotor	Stator	Rotor	Stator	Rotor	Stator
Number of blades	25	27	34	35	34	35
Mean radius (meter)	0.32	0.32	0.32	0.32	0.32	0.32
Aspect ratio	3.45	3.15	4	3.8	3.5	3.55
Hub to tip radius ratio	0.39	0.49	0.52	0.53	0.57	0.6
Rotational speed (r.p.m)	9,800	-	9,800	-	9,800	-
Tip speed (m/s)	450	-	411.3	-	398	-
Tip relative Mach number	1.63	-	1.15	-	1.08	-
Stage pressure ratio	1.55		1.36		1.25	
Stage isentropic eff.	0.944		0.9337		0.9052	

The off-design performance maps of the first rotor and the whole fan are computed and presented in figures (12) and (13). The surge margin at the design mass flow rate is then computed according to the formula introduced by [Gostelow, 1968]. As mentioned in Gostelow, the stall margin should be between 5.5% and 20%. A surge margin of 8.5% is selected for this fan at the design mass flow rate.

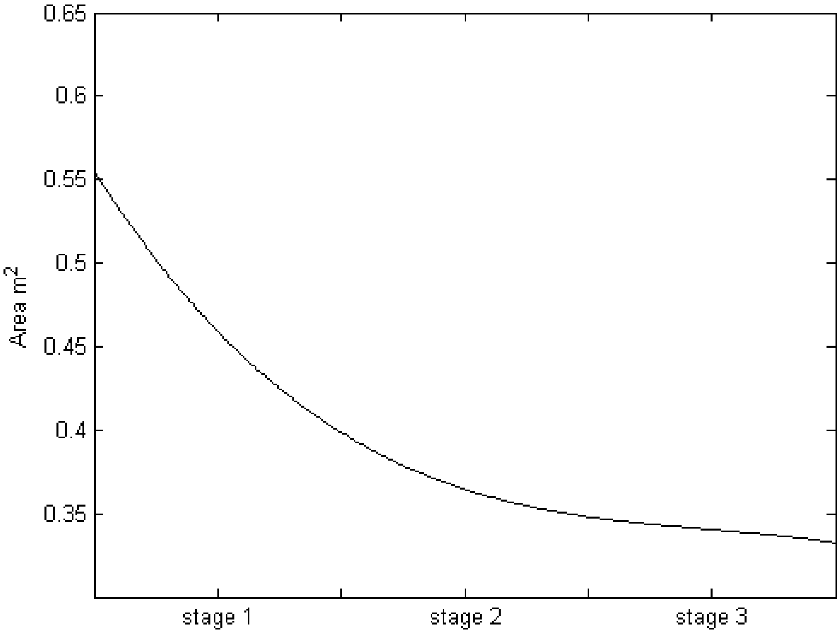

Figure 11: Annulus area distribution of the fan.

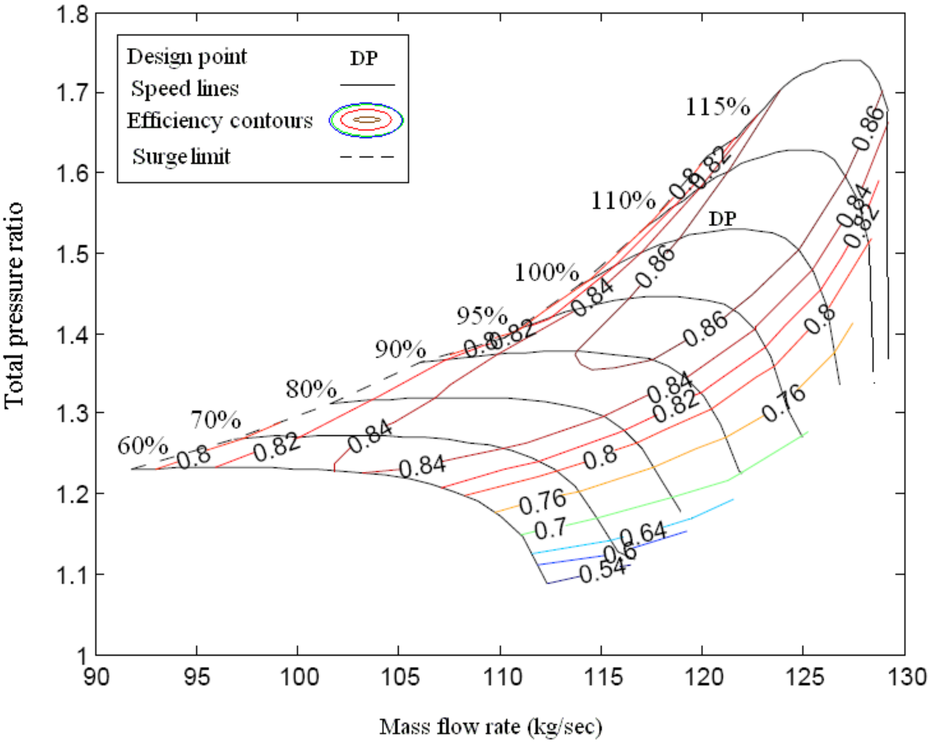

Figure 12: First rotor Performance map

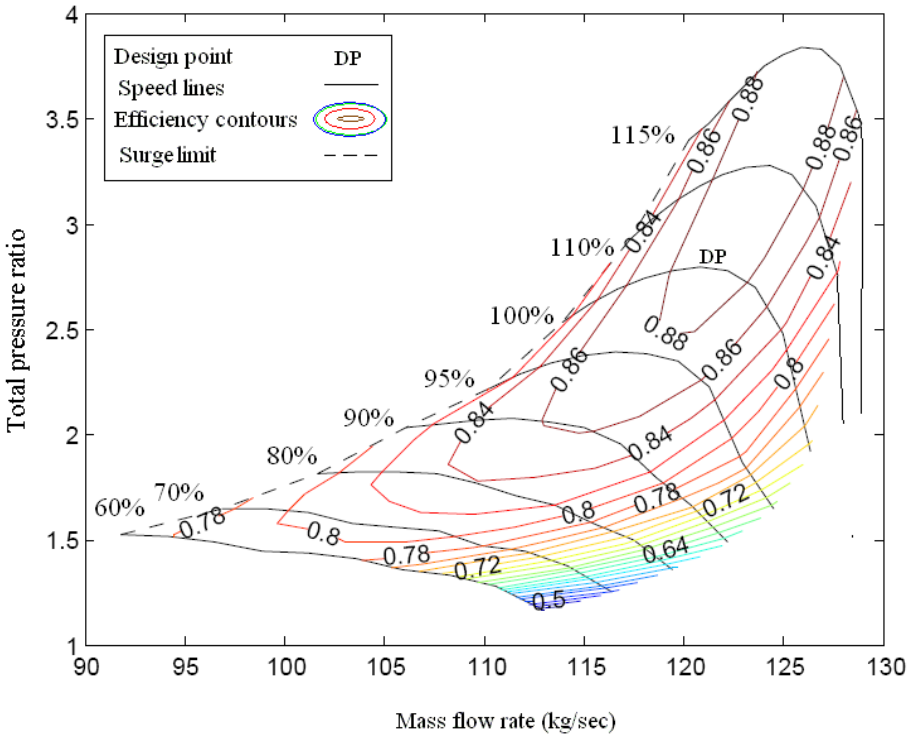

Figure 13: Overall Fan performance map

Numerical Simulations. The design shape produced by the preliminary method is simulated numerically with CFD and the results are compared with those obtained by the low fidelity method. The CFDRC-ACE multi physics module, which is a pressure based solver, is used for the numerical simulation. It solves the time-dependent, Reynolds-averaged Navier-Stokes equations for turbulent, compressible flows using a finite volume, time-marching approach on multi-zone, structured grids. Spatial accuracy is nominally second order upwind formulation. Steady flows are simulated through an iterative process using local time stepping. Turbulence is modeled using the Standard $k-\varepsilon$ model. CFD-ACE is capable of solving flows of speeds ranging from low subsonic flow to relatively high supersonic flow.

A grid sensitivity study is performed to ensure that the baseline grid has adequate sizes to resolve the solid wall boundary layers and the shock system. Simulations were conducted on different grids with variable grid points. Table 3 summarizes the sensitivity of the number of cells for structured grids. While Fig. 14 shows the variation of the observed flow quantity (i.e. total pressure ratio) for different grids with different sizes of the first grid point near the wall.

TABLE 3: Pressure ratio for different grid sizes.

No. of Cells	2E5	5E5	8E5	10 E5
1st grid spacing (meter)	8.0E-4	3.5E-4	3.0E-4	2.5E-4
(Stage Total Pressure Ratio)	1.426	1.4317	1.4327	1.4334

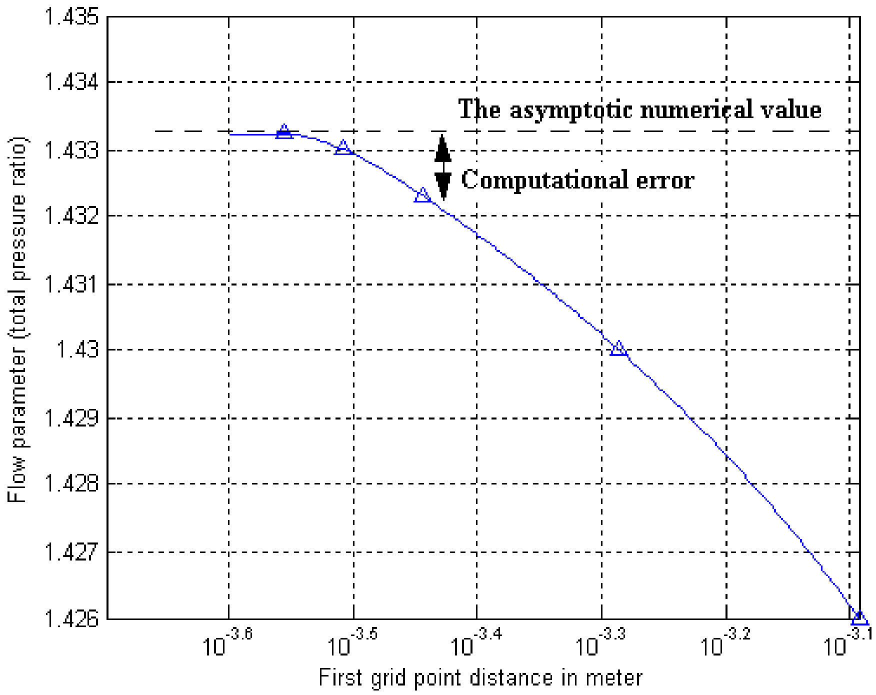

Figure 14: Effect of grid spacing on the accuracy of the steady state solution

The grid sensitivity analysis indicates that the change in the total pressure does not exceed 0.7% as the number of cells is changed from 200000 cells to 1000000 cells. In order to ensure high accuracy resolution, the structured grid has been chosen in the representation of the problem. The number of cells and the cluster factor are specified carefully to avoid having negative volumes. Figure 15 presents the baseline grid of 800,000 cells in the radial and circumferential directions that is used for the simulations. The convergence history of different flow variables is introduced in Figure 16 which indicates that the flow is converged to a steady state solution within 3000 iterations.

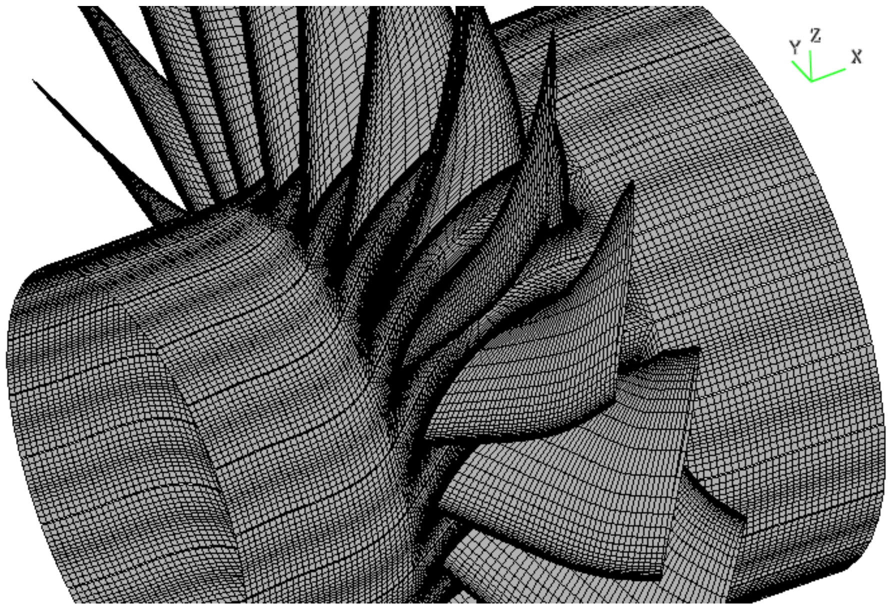

Figure 15: Baseline structured grid with 800,000 cells in the radial and circumferential directions.

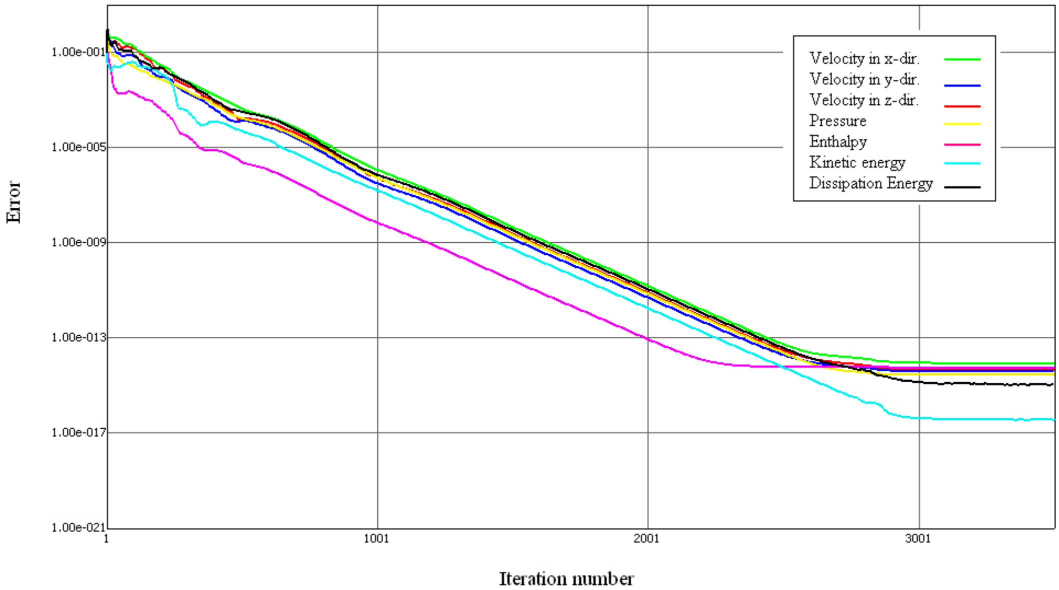

Figure 16: Convergence history

The Mach number contours at the 50% span location measured from the hub are presented in figure (17). The contours reveal that a series of oblique shock waves is formed on the blade. Thus, the total pressure ratio is increased as a result of this shock system. The rotor pressure ratio is estimated to be 1.48 as clear from figure (18) which shows the total pressure contours over the rotor inlet and outlet.

The passage shock is moved toward the blade leading edge. The shock system inside the passage is reduced to one strong shock. Some researcher explained the shape of the shock at the peak efficiency operation as an oblique shock followed by normal one [Keith M. Boyer, 2001] and [Gregory S. Bloch, 1996]. The location of the normal shock is controlled by the back pressure applied to the rotor.

Table 4 shows the axial flow compressors characteristic in the different flow regimes [Boyce, M.P, 2003]. The similar transonic stages with inlet Mach number from 0.7 to 1.1 limited by a pressure ratio from 1.15 to 1.6 and an isentropic efficiency from 80% to 85%. This values of isentropic efficiencies decreases with the increasing of the inlet relative Mach number. Which is validates the current results. The current transonic rotor shows a pressure ratio of 1.48 with absence of the stator. With the complete stage this pressure ratio should slightly decreases due to the pressure loss.

TABLE 4 Axial flow compressor characteristics [Boyce, M.P, 2003].

Type of Application (Flow)	Inlet Relative Mach Number	Pressure Ratio per Stage	Efficiency per Stage
Industrial (Subsonic)	0.4-0.8	1.05-1.2	88%-92%
Aerospace (Transonic)	0.7-1.1	1.15-1.6	80%-85%
Research (Supersonic)	1.05-2.5	1.8-2.2	75%-85%

Performance of the designed rotor during off design operation was examined. The results shows that the total pressure ratio tends to increase with the back pressure to certain value then the more back pressure increase will causes the rotor to stall Fig. 19. Decreasing the back pressure increases the isentropic efficiency to certain beak point then decreases rapidly near the choke point Fig. 20. The same trend was observed for the different operating speeds but the operation range decreases with the increase in rotor speed. This makes the operating speed to be limited to certain value. The operation range measures the stability of the rotor performance.

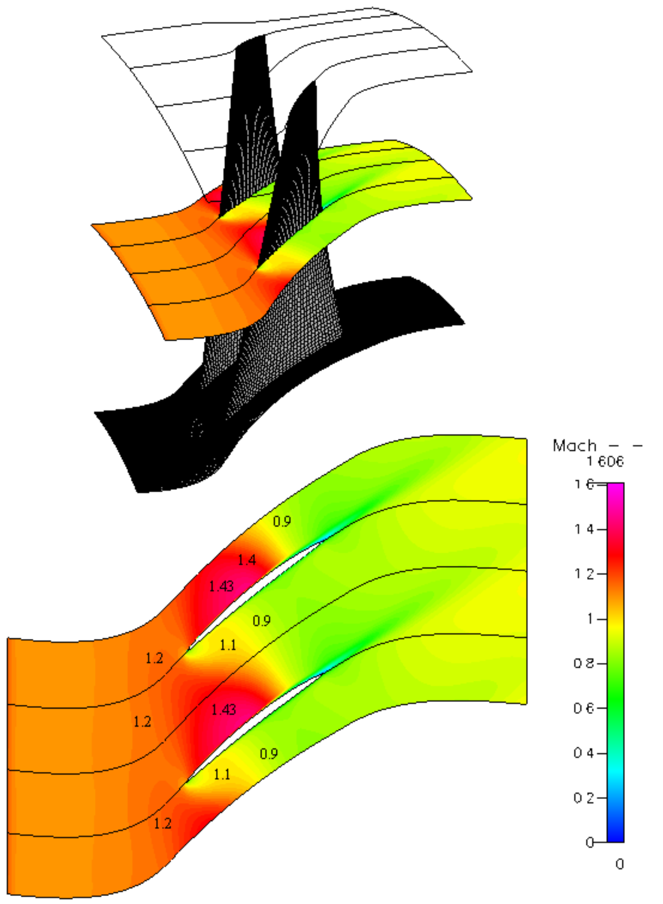

Figure 17: Mach number contours at 50 % span from hub

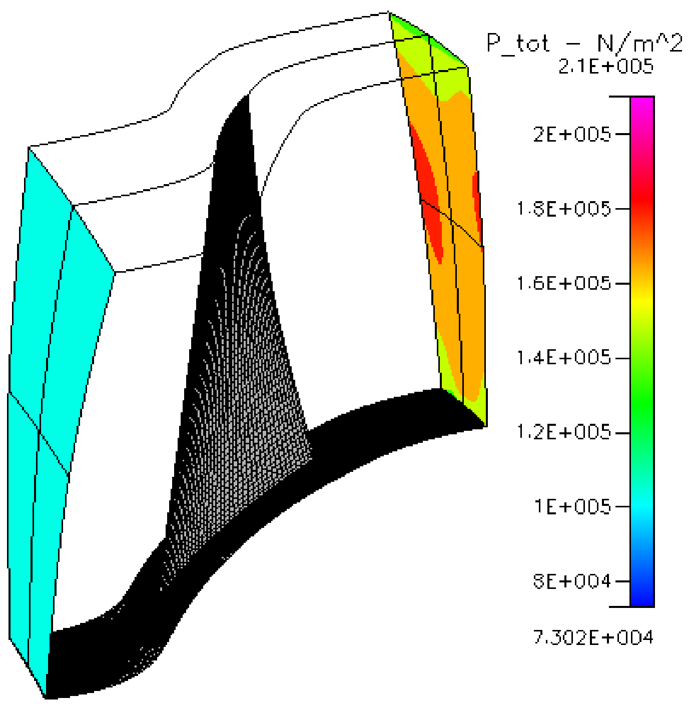

Figure 18: Inlet and outlet total pressure contours for rotor blade of the first stage.

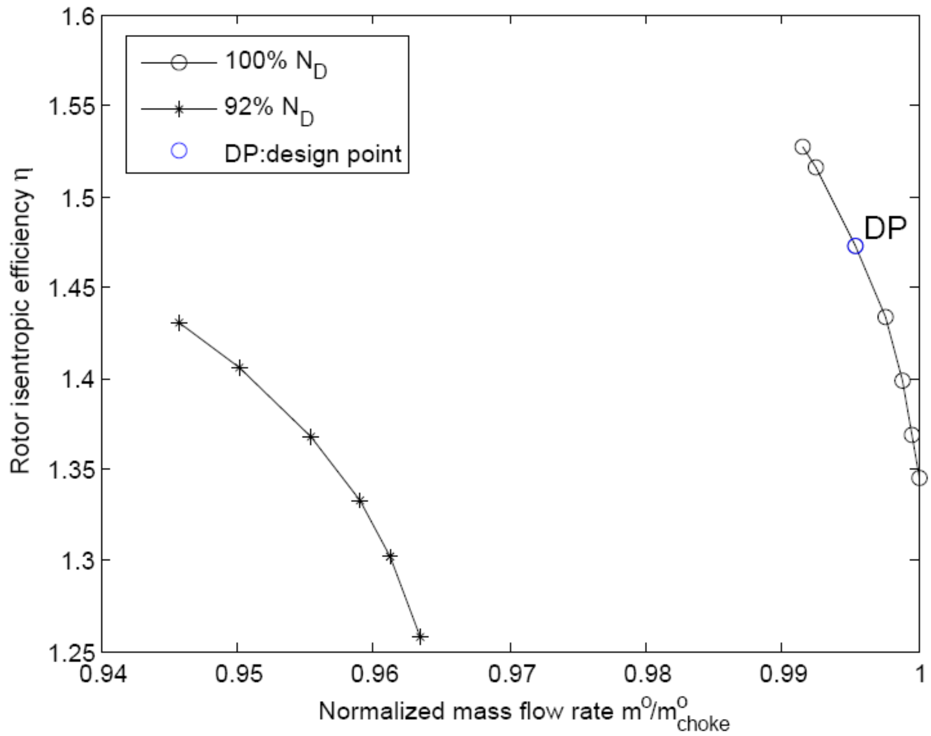

Figure 19: High fidelity design pressure ratio variation at different operating speeds.

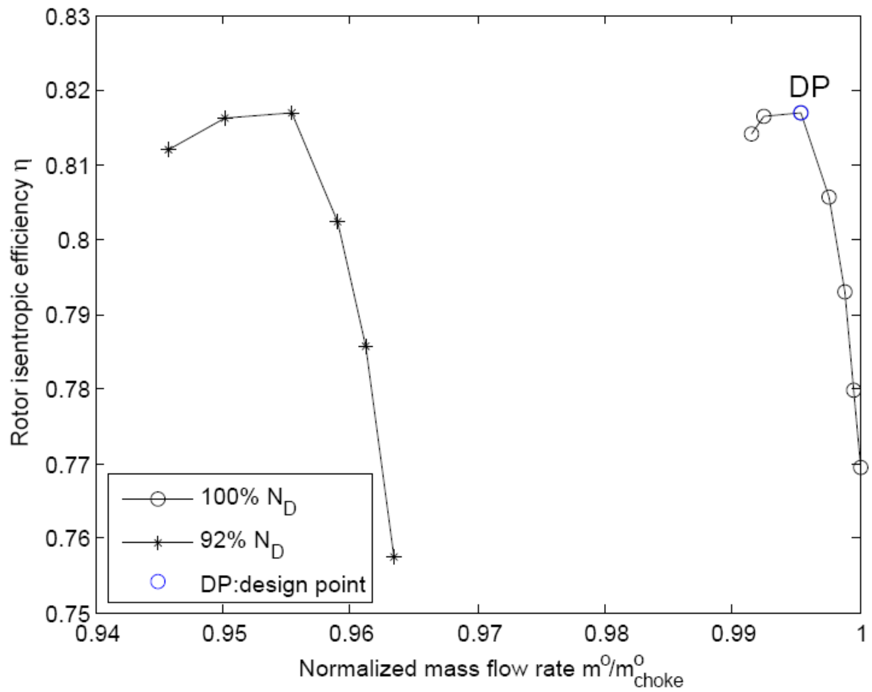

Figure 20: High fidelity design isentropic efficiency variation at different operating speeds.

The shock structure in the transonic compressor passage is very sensitive to the back pressure. There are two regimes for the back pressure controlled the number forming the shock structure, the low and high back pressure regimes [Gregory S. Bloch, 1996]. The range of back pressure for which a two distinct passage shocks exist is referred to as the "low back pressure regime". For low back pressure conditions, the passage shock which begins at the blade leading edge will be a weak shock and the flow downstream of this shock will be supersonic Fig. 21 (A). As the back pressure is increased above some "low" value, a normal shock extends across the entire passage and merges with the right branch of trailing edge Fig. 21 (B). This normal shock moves upstream with increasing back pressure and still moving until just coalesce with the first passage shock Fig. 17.

As the back pressure increased above the designed value, the normal shock continues to move upstream. The passage shock becomes a combination of a weak shock and a full passage normal shock Fig. 22 (A). If the back pressure increased above this maximum value of the "low back pressure regime" the normal passage shock will detach and moves upstream of the blade leading edge. Operating with a detached passage shock is commonly referred to as the "high back pressure" regime. Figure 22 presents the shock structure at the low and high back pressure regimes during operation.

(A) M=1.32 and P_2/P_1=1.25 (B) M=1.32 and P_2/P_1=1.4

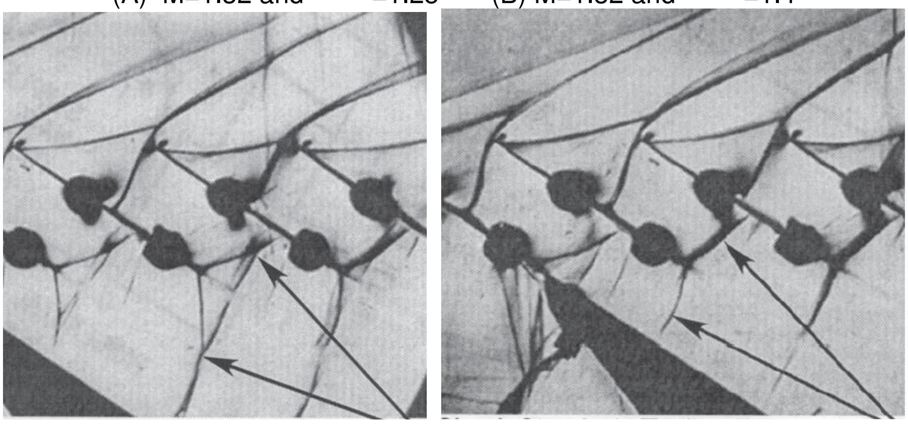

Figure 21: Variation of the second passage shock with back pressure in the low back pressure [Gregory S. Bloch, 1996]

The numerical simulations are used to validate the results obtained using the preliminary design method. The effect of the rotor stagger angle on the rotor efficiency and pressure ratio is shown in figure (23). The preliminary results shown in figure (9) are compared with those obtained using the numerical computations shown in figure (23). The numerical computations show that maximum isentropic efficiency is obtained for a rotor-stagger angle of 39^{o} which is the same result obtained using the preliminary method. In addition, the Mach number distribution through the cascade area is shown in figure (24) for stagger angles different from the design point. As the stagger angle is changed, the position of the shock wave is changed on the blade surface. Thus, the shock wave losses are affected by the setting angle of the rotor.

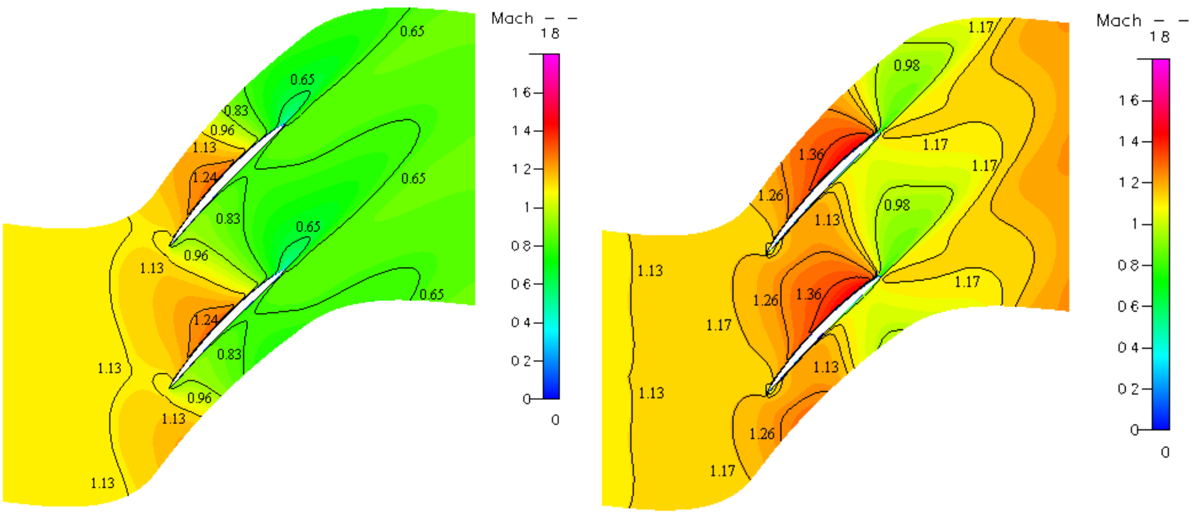

(A) Near stall (B) Near choke

Figure 22: Designed rotor Mach contours at the mean section at 100% design speed and different back pressure

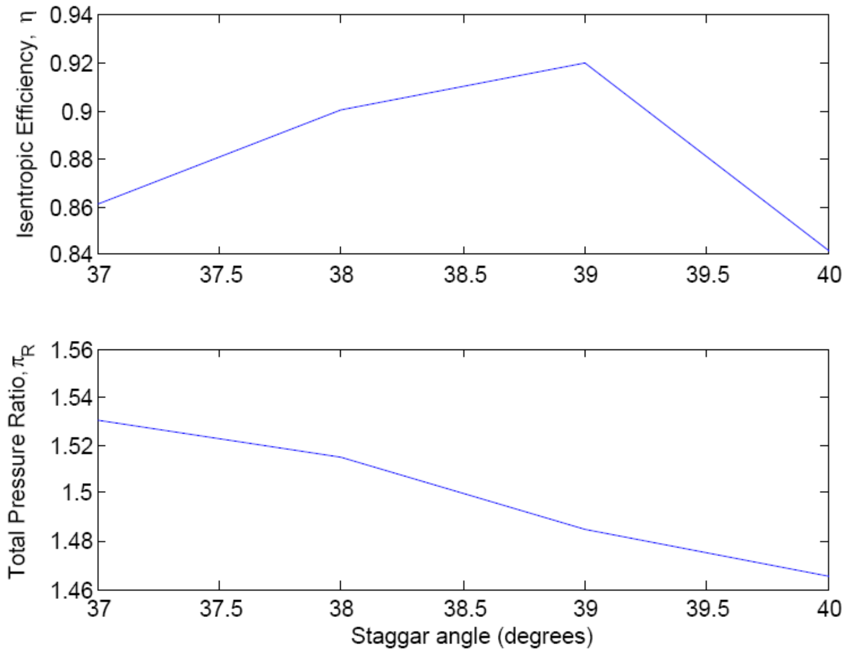

Figure 23: Variation of the total pressure ratio and isentropic efficiency with changes in rotor stagger angles

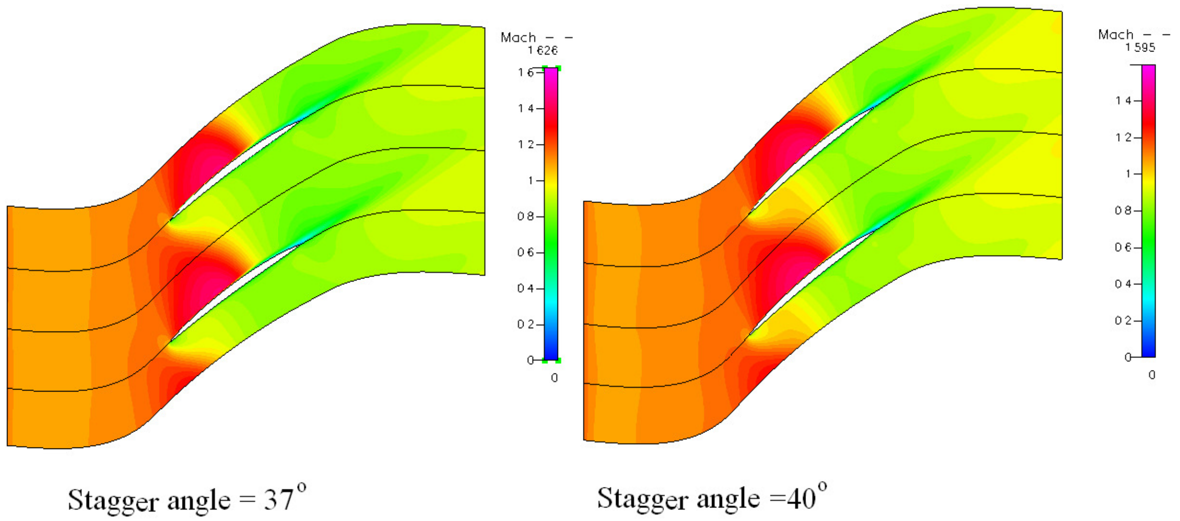

Figure 24: Mach number contours at different stagger angles of the rotor.

The effect of changing rotational speed on the rotor performance is shown in figures (25) and (26). The numerical computations indicate that maximum efficiency is obtained at the design rotational speed. This result means that good design parameters are selected using the preliminary design.

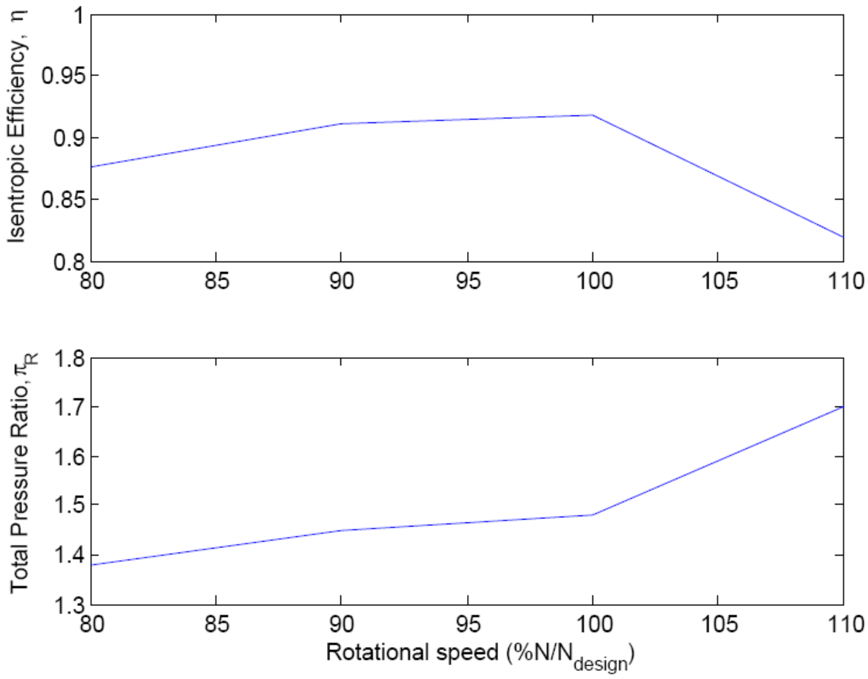

Figure 25: Variation of the total pressure ratio and isentropic efficiency with the rotational speed.

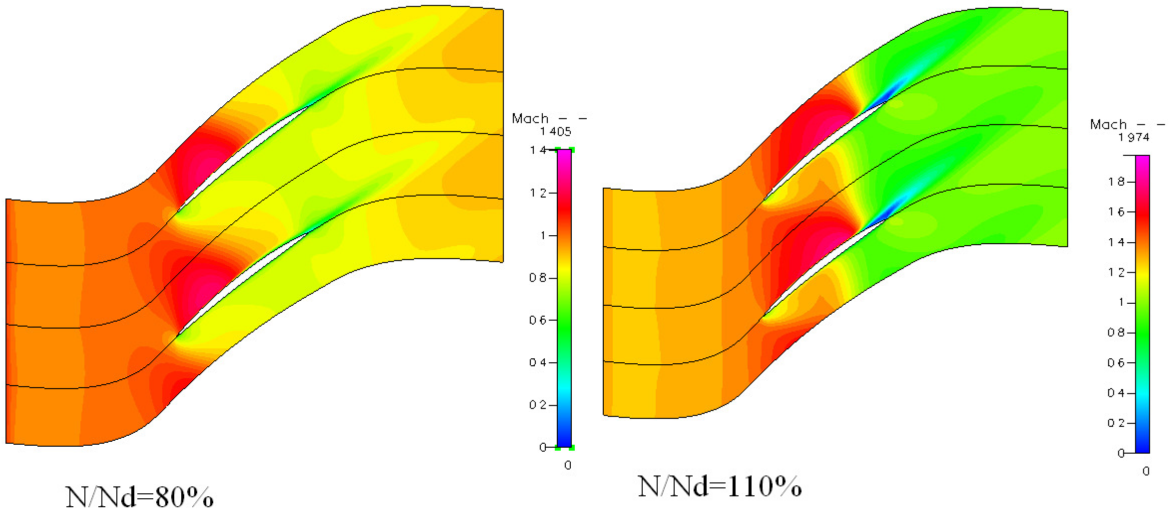

Fig. 26 Mach number contours at different rotational speeds as a percentage of the design value.

CONCLUSION

In the current study, a reliable low fidelity-design tool is developed for the design of transonic compressors. Different correlations are used to predict the shock wave losses, profile losses, deviation angle and the design incidence. The developed tool is used to compute an initial geometry for the numerical simulations. A parametric study of compressor blade geometry is performed to achieve optimum design and off-design operations in terms of fan efficiency and surge margin. The blade geometry is defined in terms of five parameters for a multiple circular arc MCA-profile. In addition, a parametric study is performed on the stagger angles and the rotational speed. The off design operation of the design shape produced by the preliminary method is performed with CFD. The parametric study is also simulated numerically with CFD and the results are compared with those obtained by the low fidelity method. The CFDRC-ACE is used for the numerical simulation. The results computed numerically prove that good design parameters are selected using the preliminary method.

NOMENCLATURE

A = *Area,* (m^2)
c = *chord length, (m)*
D =*Diffusion factor*
DCA =*Double circular arc*
i =*Incidence angle*
LER =*Leading edge raduis*
$\dot{m}$ = *Mass flow rate,* (kg/s)
M =*Mach number*
MCA = *Multiple circular arc*
N = *Rotational speed, (r.p.m)*
P = *Total pressure, (Pa)*
r = *Radius, (m)*
R = *Normalized radius, r/rm*
T = *Total Temperature, (K)*
t =*Blade thickness*
U = *Tangential speed, (m/s)*
W = *Relative flow velocity, (m/s)*

Greek Symbols

α = *Air angle, (degrees)*
β = *Blade angle*
γ =*Ratio of specific heats*
Γ =*Blade row circulation*
θ =*Boundary layer momentum thickness*
ρ =*Density (kg/m3)*
σ =*Solidity, c/s*
ω =*Total pressure loss*
η = *Efficiency*
λ = *Work done factor*
π = *Pressure ratio*
ζ =*Stagger angle*
ψ =*Angle between shock surface and upstream flow*

Subscripts

a = *axial*
f = *fan*
h = *hub*
m = *mean*
t = *tip*
θ = *tangential*
1 = *Rotor inlet*
2 = *Rotor outlet*

REFRENCES

B. Lakshminarayana and J. H. Horlock, (1963). Tip Clearance Flow and Losses for an Isolated Compressor Blade. Aeronautical Research council reports and memoranda, London, 1963.

Boyce, M.P,(2003), Gas Turbine Engineering Handbook, Second Edition, Butterworth-Hienemann 2003.

Carter, A.D.S. Hughes,.H.P. (1950), "A Theoretical Investigation into the Effect of Profile Shape on the Performance of Aerofoils in Cascade, ARC Rep. and Memo. 2384.

Creveling, H.F.,(1968), “Axial-Flow Compressor Computer Program for Calculating Off-Design Performance,” NASA CR 72472.

Cetin, M., Ucer, A.S., Hirsch, Ch., and Serovy, G.K., (1987) “Application of Modified Loss and Deviation Correlations to Transonic Axial Compressors” AGARD Report No. 745 Novembe.

Chen, N.; Zhang, H.; Xu, Y. & Huang, W. (2007). Blade Parameterization and Aerodynamic Design Optimization for a 3D Transonic Compressor Rotor, Journal of Thermal Science, Vol. 16, No. 2, (May 2007), pp. 105-114, ISSN 1003-2169.

Cumpsty, Nicholas A.(1989) Compressor Aerodynamics. New York: John Wiley & Sons, Inc.

Freeman, C. & Cumpsty, N. A. (1992). Method for the Prediction of Supersonic Compressor Blade Performance, Journal of Propulsion and Power, Vol. 8, No. 1, (Jan-Feb 1992), pp. 199-208, ISSN 0748-4658.

Gregory S. Bloch, (1996)," Flow Losses in Supersonic Compressor Cascades"", Doctor of Philosophy, Virginia Polytechnic Institute and State University , Blacksburg, Virginia, July 1996.

Hah, C. & Reid, L. (1992). A Viscous Flow Study of Shock-Boundary Layer Interaction, Radial Transport, and Wake Development in a Transonic Compressor, ASME Journal of Turbomachinery, Vol. 114, No. 3, (July 1992), pp. 538-547, ISSN 0889-504X.

Hearsey, R.M.,(1970) “HT0300-A Computer Program for the Design and Analysis of Axial Turbomachinery,” Parts I-II, Cambridge, Massachusetts, March 1970.

H.I.H. Saravanamuttoo, GFC Rogers and H Cohen, (2001),”Gas Turbine Theory”, Prentice Hall, 5th Edition.

J. H. Horlock, (1973), "Axial flow compressors, fluid Mechanics and Thermodynamics", Ropert E. Krieger Publishing Company, 1973.

J.P. Gostelow, K.W. krabacber, L.H. Smith, Jr. (1968) "Performance Comparisons of High Mach Number Compressor Rotor Blading", Nationnal Aerodynamics and Space Administration.Washington, D.C. Decembe.

Joseph E. Cahill (1997)" Identification and Evaluation of Loss and Deviation Models for use in Transonic Compressor Stage Performance Prediction", Master of Science, Virginia Polytechnic Institute and State University , Blacksburg, Virginia, September 22, 1997.

König, W.M., C.K. Hennecke, and L. Fottner. “Improved Blade Profile Loss and Deviation Angle Models for Advanced Transonic Compressor Bladings: Part II – A Model for Supersonic Flow,” ASME Journal of Turbomachinery, 117 :81–87 (January 1996).

Koch, C.C., Smith, L.H., (1976,) “Loss Sources and Magnitudes in Axial-Flow Compressors,” ASME Journal of Engineering for Power, Vol. 98, 1976, pp. 411-424.

Keith M. Boyer, (2001)" An Improved Streamline Curvature Approach for Off-Design Analysis of Transonic Compression Systems", Doctor of Philosophy, Virginia Polytechnic Institute and State University , Blacksburg, Virginia, April 2001.

Law and Puterbaugh, (1988)" Parametric Blade Study Test Report Rotor Configuration. Number 1", Air force wright aeronautical labs Wright-Patterson AFB OH, Nov 1988.

Lieblein, S.(1965), “Viscous Flow in Two-dimensional Cascades,” NASA SP-36, 1965.

Miller, G. R.; Lewis, Jr., G. W. & Hartmann, M. J.(1961) , Shock Losses in Transonic Compressor Blade Rows, ASME Journal of Engineering for Power, Vol. 83, No. 3, July 1961, pp. 235-242.

Moeckel, W.E.,(1949) “Approximate Method for Predicting Form and Location of Detached Shock Waves Ahead of Plane or Axially Symmetric Bodies,” NACA TN 1921, 1949.

Ning, F. & Xu, L. (2001). Numerical Investigation of Transonic Compressor Rotor Flow Using an Implicit 3D Flow Solver With One-Equation Spalart-Allmaras Turbulence Model, Proceedings of ASME Turbo Expo 2001, 2001-GT-0359.

Puterbaugh, S. L.; Copenhaver, W. W.; Hah, C. & Wennerstrom, A. J. (1997). A Three- Dimensional Shock Loss Model Applied to an Aft-Swept, Transonic Compressor Rotor, ASME Journal of Turbomachinery, Vol. 119, No. 3, (July 1997), pp. 452-459, ISSN 0889-504X

R. Mdouki, A. Gahmousse, (2012) " Numerical Exploration of Endwall Flow in a Slotted Compressor Cascade at Design Condition", International Review of Aerospace Engineering, March 2012 (Part A), Vol. 6 N. 3, pp. 520-527.

Roberto Biollo and Ernesto Benini (2011). "State-of-Art of Transonic Axial Compressors, Advances in Gas Turbine Technology", Dr. Ernesto Benini (Ed.), ISBN: 978-953-307-611-9, InTech.

Schreiber, H.-A., and Tweedt, D. L., (1987), "Experimental Investigation and Analysis of the Supersonic Compressor Cascade ARL-2DPC," DFVLR IB-325-02-87.

Strazisar, A. J. (1985). Investigation of Flow Phenomena in a Transonic Fan Rotor Using Laser Anemometry, ASME Journal of Engineering for Gas Turbines and Power, Vol.107, No.2, (April 1985), pp. 427-435, ISSN 0742-4795

Suder, K. L.; Chima, R. V.; Strazisar, A. J. & Roberts, W. B. (1995). The Effect of Adding Roughness and Thickness to a Transonic Axial Compressor Rotor, ASME Journal of Turbomachinery, Vol. 117, No. 4, (October 1995), pp. 491-505, ISSN 0889-504.

Wadia, A. R. & Law, C. H. (1993). Low Aspect Ratio Transonic Rotors: Part 2-Influence of Location of Maximum Thickness on Transonic Compressor Performance, ASME Journal of Turbomachinery, Vol. 115, No. 2, (April 1993), pp. 226-239, ISSN 0889-504X.

Wennerstrom, A. J. & Puterbaugh, S. L. (1984). A Three-Dimensional Model for the Prediction of Shock Losses in Compressor Blade Rows, ASME Journal of Engineering for Gas Turbines and Power, Vol. 106, No. 2, (April 1984), pp. 295-299, ISSN 0742-4795

Wennerstrom, Arthur. J.(2000.), Design of Highly Loaded Axial-Flow Fans and Compressors, Concepts ETI, Inc, 2000.

Wu, C. H., (1952) A General Theory of Three-Dimensional Flow in Subsonic and Supersonic Turbomachines of Axial-, Radial-, and Mixed Flow Types, NACA TN 2604, 1952.